nature research

https://doi.org/10.1038/s41565-020-00789-w

Supplementary information

Observation of single-defect memristor in an MoS_2 atomic sheet

In the format provided by the authors and unedited

Observation of Single-defect Memristor in an MoS_2 Atomic Sheet

Saban M. Hus, Ruijing Ge, Po-An Chen, Liangbo Liang, Gavin E. Donnelly, Wonhee Ko, Fumin Huang, Meng-Hsueh Chiang, An-Ping Li, and Deji Akinwande*.

Supplementary Information

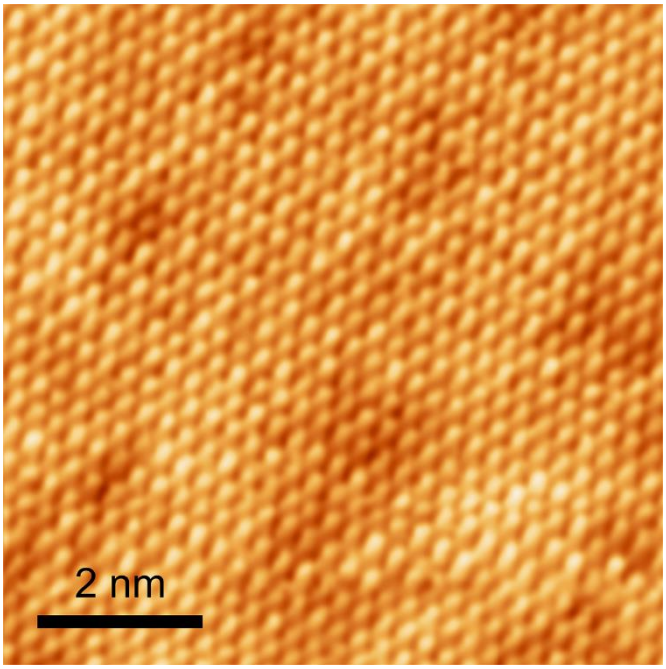

Supplementary Fig. 1 | STM image of high quality exfoliated MoS_2 monolayers. STM images show that MoS_2 monolayers have very low defect density after annealing at 250°C.

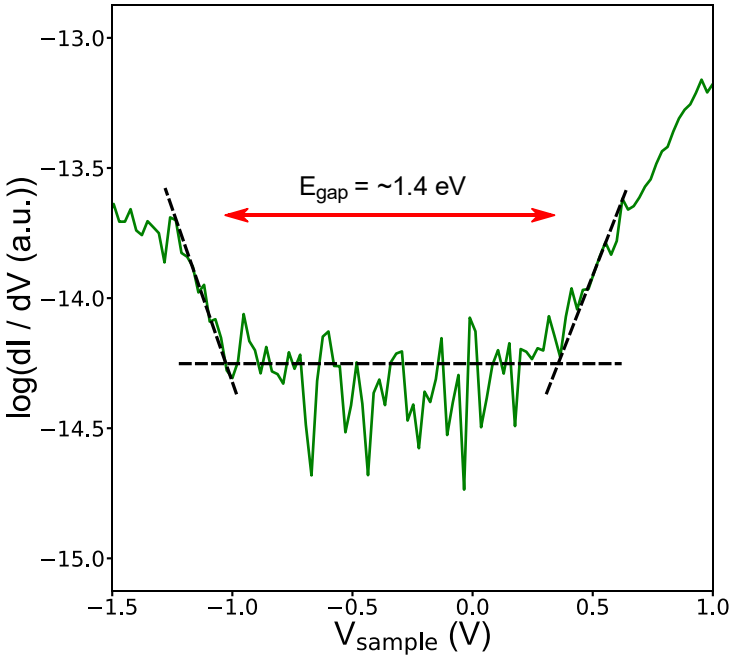

Supplementary Fig. 2 | Typical STS spectra on defect free regions and determination of the bandgap. STS of MoS_2 monolayers on gold film presents a reduced bandgap and n-type doping due to charge transfer from underlying gold substrate. The bandgap values are determined by interpolating the exponential decay of dI/dV curves.

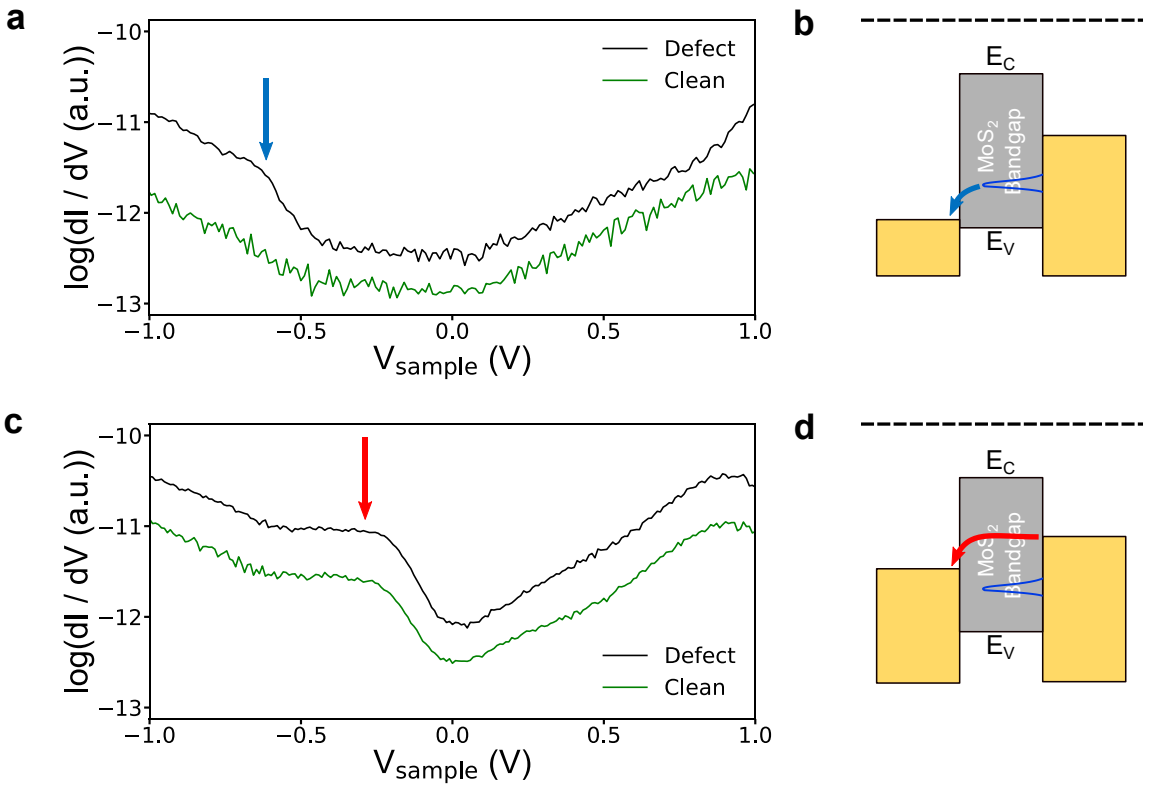

Supplementary Fig. 3 | Tunneling spectra and band diagrams for the tip–MoS_2–Au junction. a, STS spectra for stabilization voltage close to the edge of the band gap of MoS_2 (V_{sample}=-1.0V). **b,** Illustrates the band diagram where the vacuum gap is significantly reduced and tunneling from MoS_2 defect states (blue arrow) are dominant. **c,** STS spectra for stabilization voltage inside the band gap of MoS_2 (V_{sample}= -0.5V). **d,** In this case the tip contacts the sample, and direct tunneling from Au states (red arrow) dominate the total current. STS spectra are shifted vertically for clarity.

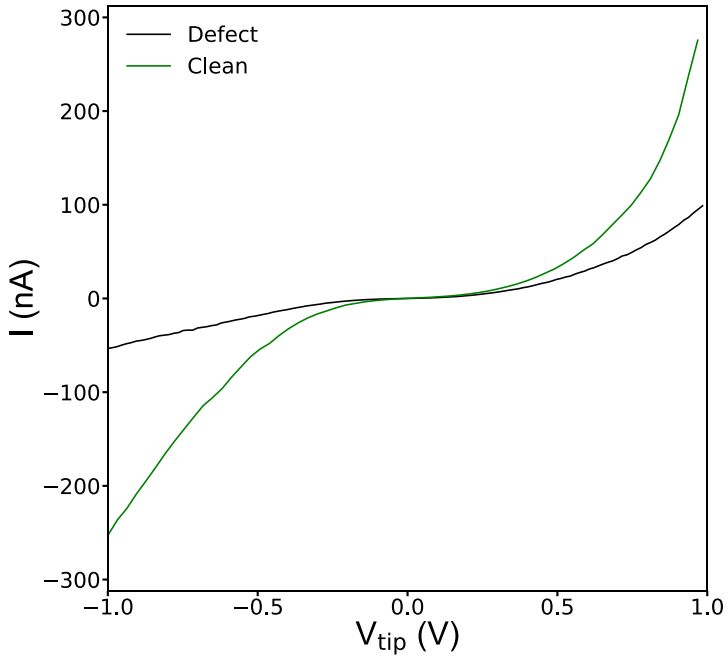

Supplementary Fig. 4 | Transport measurements with longer tip approaching. Representative I-V curves with tip approach of 0.35 nm and no switching event.

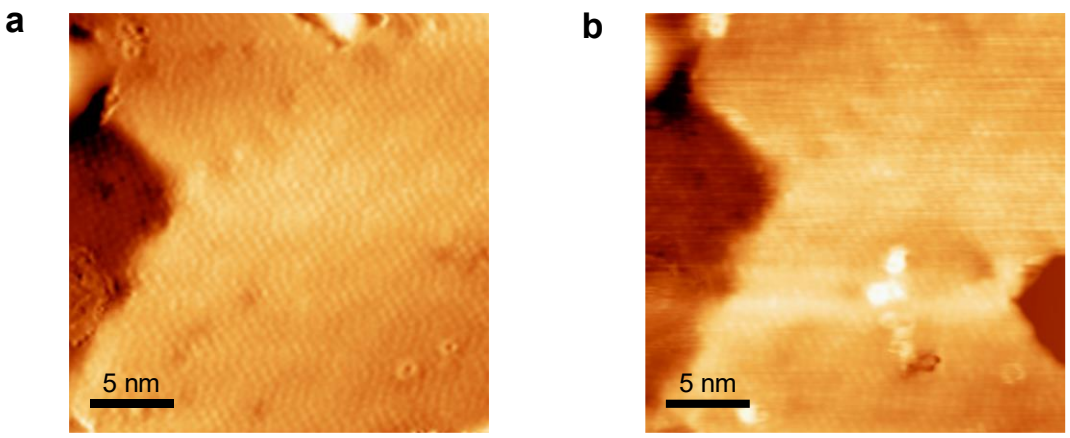

Supplementary Fig. 5 | Atomic resolution STM image of a defect site before and after a switching event. a, Defect site before switching event. **b,** The same defect site after switching event**.**

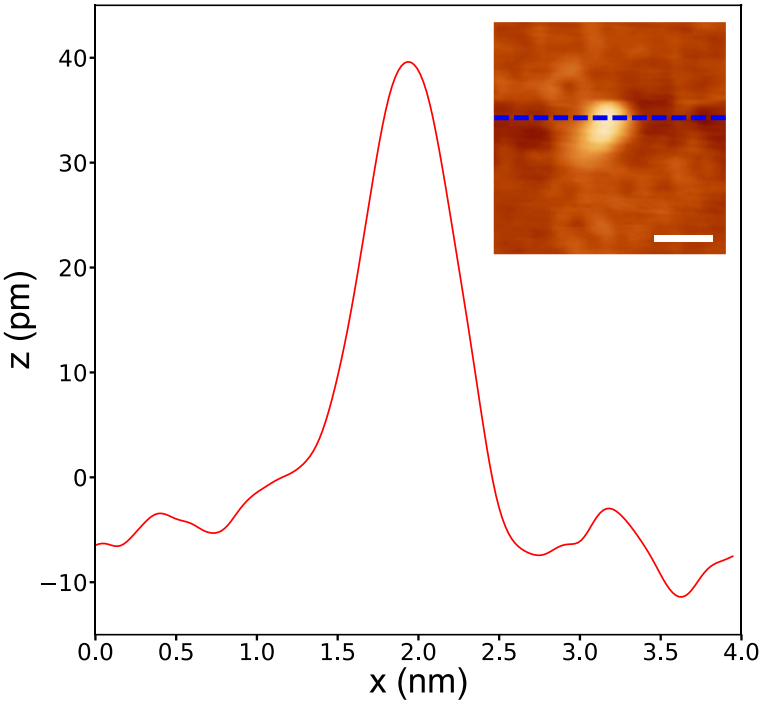

Supplementary Fig. 6 | STM height profile at the Au absorbed V_{S2} defect site. Inset: STM image of Au absorbed V_{S2} defect site. Scale bar: 1nm. Height profile along the dashed blue line shows a protrusion of about 50 pm indicating a substitution like defect rather than an adatom. The Au atom migrates to the defect site from the gold STM tip due to strong electric field at the tip apex.

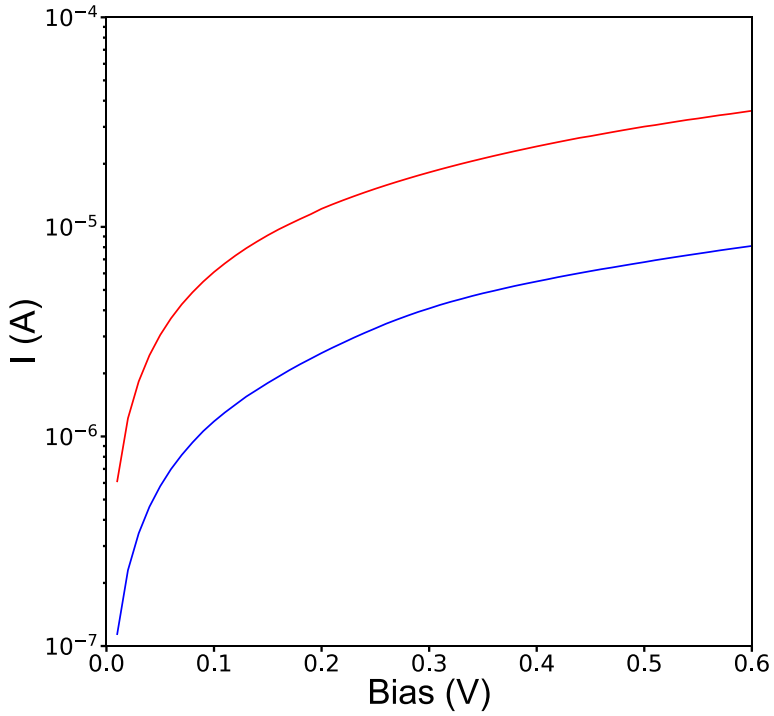

Supplementary Fig. 7 | Calculated I-V curves of two first-principles simulated device structures. Pristine (blue line) and with single gold adsorption into staggered sulfur divacancy (red line). The calculation shows increased current owing to gold adsorption consistent with experimental observation. The GGA method overestimates the OFF current due to the known underestimation of the bandgap by this technique, resulting in a reduced on/off ratio. More precise quantitative I-V can be obtained using HSE functionals in lieu of GGA, a matter of further research.

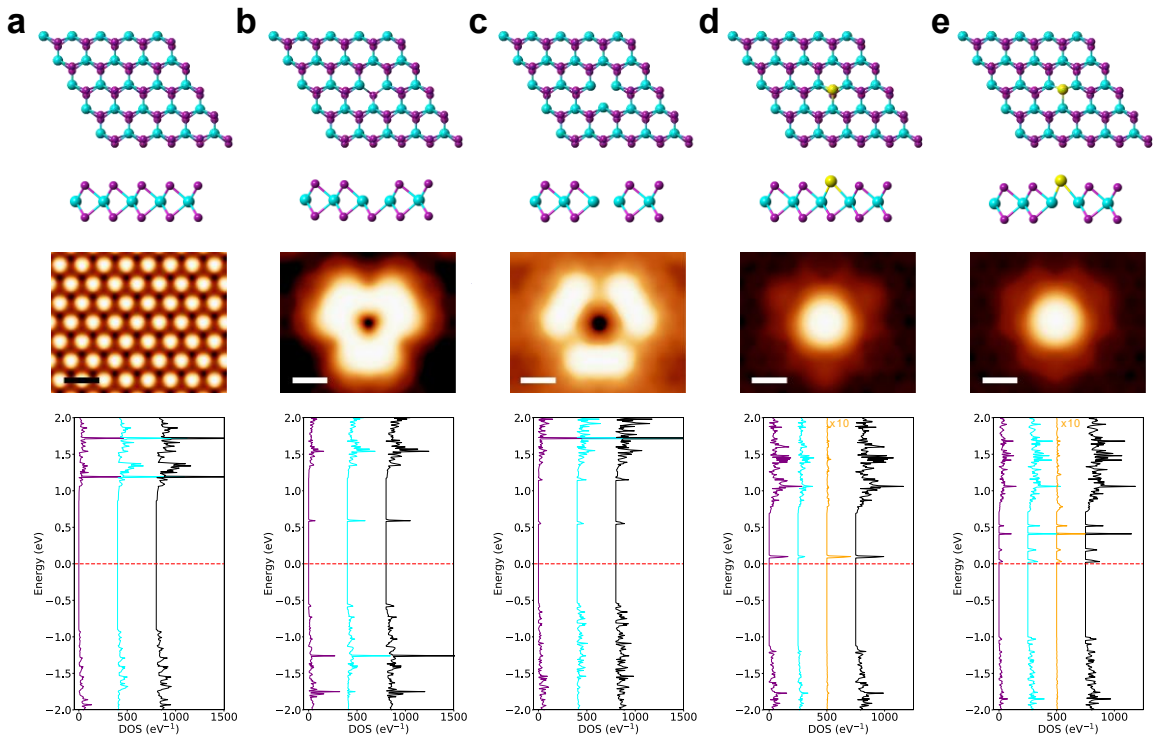

Supplementary Fig. 8 | Crystal structure, simulated STM images and LDOS for various MoS_2 defects. Top view (top row), and cross-sectional view (second row) of crystal structure for various defects. Simulated STM images (third row) and calculated LDOS (bottom row) for these structures. Purple represents S, Cyan represents Mo, and Yellow represents Au atoms in the structure images and LDOS plots. Black spectra represent total LDOS, and dashed red lines represent the Fermi level. Scale bars:0.5 nm. **a,** pristine MoS_2. **b,** monovacancy (V_S) defect. **c,** divacancy (V_{S2}) defect. **d,** Au substituted V_S defect. **e,** Au substituted V_{S2} defect. Individual spectra are shifted for clarity.

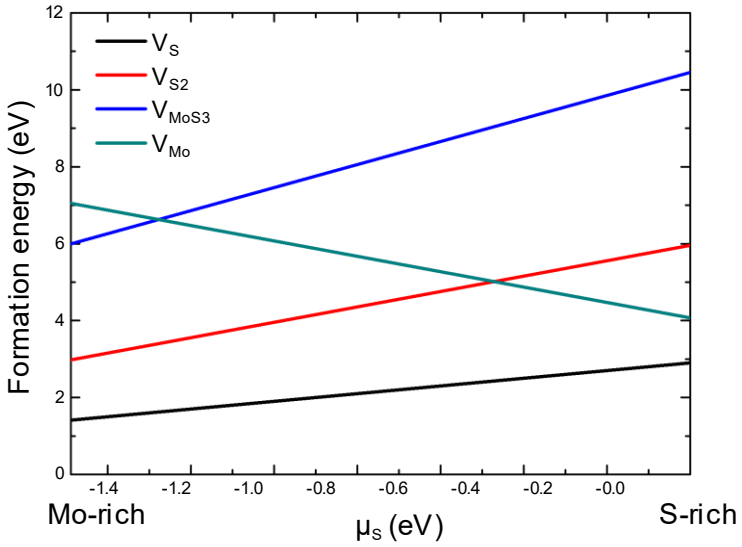

Supplementary Fig. 9 | Formation energy for various MoS_2 defects. V_S defects has the lowest formation energy followed by the V_{S2} defects.